

Article

Experimental and Numerical Analysis of Reinforced Concrete Columns under Lateral Impact Loading

Airon Chen ¹, Yanjie Liu ¹, Rujin Ma ^{1,*} and Xiaoyu Zhou ²¹ Department of Bridge Engineering, Tongji University, Shanghai 200092, China² Shanghai Urban Construction Design & Research Institute Co., Ltd., Shanghai 200125, China

* Correspondence: rjma@tongji.edu.cn

Abstract: Reinforced concrete bridge columns (RCCs) are vulnerable to collisions with vehicles or vessels. To assess the performance of RCCs under lateral impact loading and to guide the impact-resistant design of RCCs, scaled model tests and numerical simulations were carried out in this study. An experimental facility was designed, and three sets of RCC specimens were tested. The specimens were available in three sizes: 60 cm × 14 cm × 14 cm, 80 cm × 14 cm × 14 cm, and 80 cm × 20 cm × 20 cm. Finite element models of RCCs were created in LS-DYNA, and parametric studies were carried out to investigate the variables influencing the impact resistance of RCCs. According to the findings, the impact mass and velocity had a positive correlation with the extreme value of dynamic strain. When the mass of a model car increased by 22.8% and 45.6% during the impact test, the extreme concrete strain at the same position increased by 22.5% and 42.3%, respectively. In addition, as the longitudinal reinforcement ratio increased, RCCs exhibited significantly less plastic deformation and damage. The findings of this study aided in the formulation of several recommendations for future research.

Keywords: reinforced concrete columns; impact test; numerical simulation; failure mode



Citation: Chen, A.; Liu, Y.; Ma, R.; Zhou, X. Experimental and Numerical Analysis of Reinforced Concrete Columns under Lateral Impact Loading. *Buildings* **2023**, *13*, 708. <https://doi.org/10.3390/buildings13030708>

Academic Editor: Oldrich Sucharda

Received: 7 February 2023

Revised: 28 February 2023

Accepted: 6 March 2023

Published: 8 March 2023



Copyright: © 2023 by the authors. Licensee MDPI, Basel, Switzerland. This article is an open access article distributed under the terms and conditions of the Creative Commons Attribution (CC BY) license (<https://creativecommons.org/licenses/by/4.0/>).

1. Introduction

Reinforced concrete columns (RCCs) play an important role in bridges by supporting vertical loads from upper structures. They are also vulnerable to lateral impact loads caused by vehicle or vessel collisions. Figure 1 shows the damage to a bridge pier on IH-37 in Texas caused by a truck–tractor collision on 14 May 2004 [1]. On 15 June 2007, a vessel collided with the Jiujiang Bridge in China [2]. After two nearby piers collapsed, the bridge deck fell into the river (Figure 2).

The response of RCCs to transient impact loads differs significantly from that of traditional static loads. Since Abrams [3] discovered that the compressive strength of concrete is rate-sensitive in material dynamics experiments, numerous studies on the rate-related behavior of concrete materials have been conducted. It has been discovered that strain rate affects the mechanical behavior of concrete in a wide range of situations [4–8]. According to these studies, as the strain rate increases, the dynamic load strength of concrete specimens increases nonlinearly.

A variety of research methods, including experimental, analytical, and numerical investigations, have been used to investigate the behavior of reinforced concrete components under impact loads. Most previous experiments in the field have used drop hammer impact to investigate the dynamic responses of reinforced concrete structural members, such as beams, slabs, and columns [9–12]. Due to the difficulty of carrying out impact tests, numerical simulation has emerged as an important tool for analysis [13,14]. When RCCs are impacted in various locations, they can experience localized failure modes and damage, such as brittle spalling, scabbing, perforation, and punching shear failure, as well as overall flexural failure modes [15–22]. The impact-resistant behaviors of columns differ from those of the beams due to axial load. Previous research has found that the failure modes of RCCs

with axial loads are not thoroughly explained, and more research is required to understand the mechanism underlying it.



Figure 1. Bridge pier under vehicle collision [1].



Figure 2. Bridge pier under vessel collision [2].

In this study, an experimental facility was designed to facilitate the application of axial pressure on RCCs. This paper aims to first clarify the failure mechanism of RCCs under lateral impact loading through experimental and numerical research and then to evaluate the key factors affecting the impact resistance of RCCs by a parametric analysis. Firstly, an experimental facility is designed, and three sets of RCC specimens are tested. An analysis is conducted on how the response of RCCs under lateral impact loading is affected by impact energy, boundary conditions, and axial pressure. Secondly, finite element models of the RCCs are created in LS-DYNA. By contrasting simulation results with experimental data, the validity of the numerical simulation method and constitutive material model are established. Finally, parametric studies are carried out to investigate the variables influencing the impact resistance of RCCs.

2. Impact Test

2.1. Experimental Facility

When studying lateral impact, the drop hammer device is a common test device used in the medium- and low-strain-rate ranges. However, providing the initial axial pressure, which is significantly correlated with failure mode and impact resistance, proves difficult. In this study, an experimental facility (Figures 3 and 4) was designed to facilitate the application of axial pressure, and a scaled model experiment was conducted.

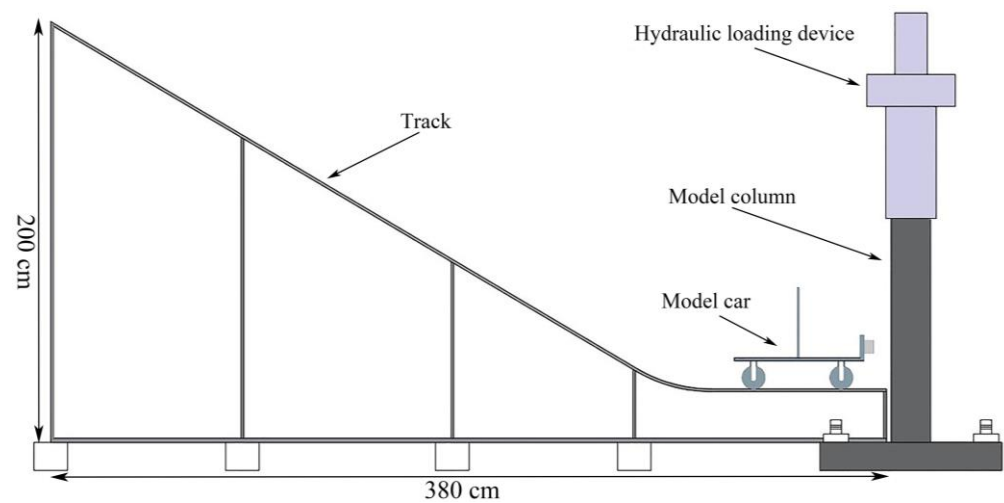


Figure 3. Schematic diagram of the experimental facility.

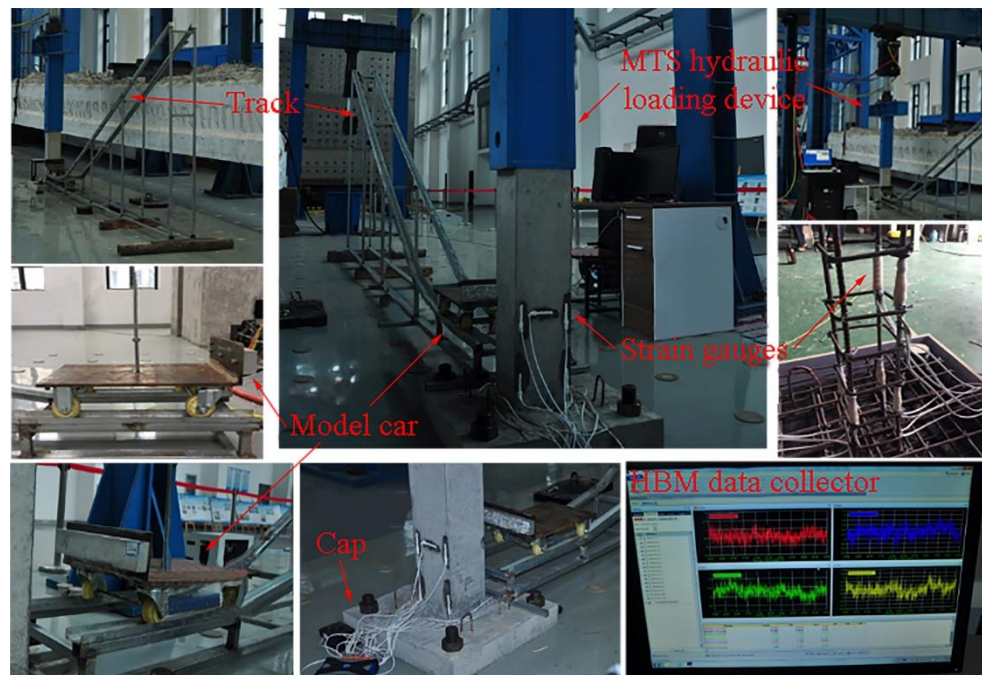


Figure 4. Experimental facility and signal acquisition system.

To obtain different impact velocities, a model car was released at various heights along the track. The track was made of U-shaped aluminum alloy and measured 200 cm in height and 380 cm in horizontal length. It was made up of three sections: a linear acceleration section, a horizontal straight section, and an arc transition section. Steel plate and roller bearings were used to construct the model car. An aluminum block for impact was fixed on the head of the car. The weight of the empty car was 17.55 kg, which could be added to with the car's fixing screw. An MTS hydraulic loading device was used to load the axial pressure of the column. A reinforced concrete cap was designed at the bottom of the model column and fastened to the laboratory reaction floor via designated anchor holes. Two strain gauges were pre-buried at the same measuring point in case either of them failed to function during the concrete-pouring and maintenance process. For signal acquisition, an HBM MX1601B data collector was used.

2.2. Reinforced Concrete Column Specimens

Three RCC specimens were manufactured and tested in this study (Figure 5). The dimensions of C_1 were 60 cm by 14 cm by 14 cm. The dimensions of C_2 were 80 cm by 14 cm by 14 cm. The dimensions of C_3 were 80 cm by 20 cm by 20 cm. C30 concrete was used, and four $\Phi 8$ steel bars were arranged longitudinally. HPB235 stirrups were arranged as $\Phi 6@5$ cm. A BX120-5AA strain gauge was affixed to the longitudinal rebar and covered with a waterproof layer, and a BX120-50AA strain gauge was affixed to the concrete. With four anchor holes set aside, the reinforced concrete cap had dimensions of 65 cm by 65 cm by 10 cm. The three concrete standard test blocks were simultaneously conserved in order to determine the mechanical characteristics of the concrete material. The strengths of the test blocks were 34.2 MPa, 35.8 MPa, and 37.3 MPa.

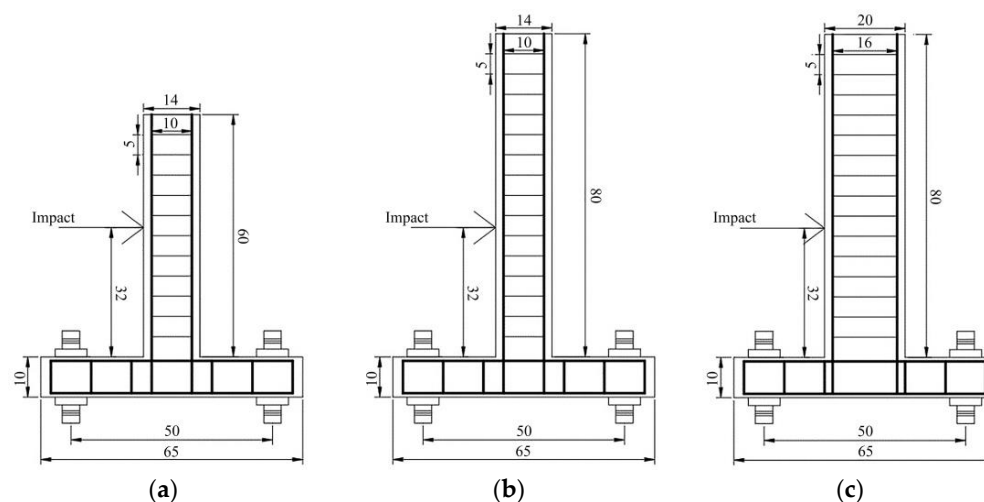


Figure 5. Dimensions of RCC specimens (unit: cm): (a) C_1; (b) C_2; (c) C_3.

During the experiment, the following measurements were collected: (1) the concrete vertical and transverse strains on the backside of the impact location; (2) the rebar vertical strain on the backside of the impact location; and (3) the concrete and rebar vertical strains at the bottom. The validity of the strain gauge at the measuring point was checked before the experiment.

2.3. Experimental Procedure

In the impact test, the model car was dropped and accelerated from four different heights to hit the fixed model column in the straight section of the track. A dynamic data collector was used to collect the strain data of the rebar and concrete. The impact velocity was calculated by referring to the video recorded.

To investigate the typical failure modes of RCCs under lateral impact loads and the critical variables influencing the transition to failure mode, two sets of cantilever column impact tests were carried out. Due to the high risk of failure under large axial pressure, the degree of damage to the model column at the maximum impact energy was previously examined using numerical simulation to ensure the experiment's safety.

The model column section, impact kinetic energy, and axial pressure were considered to determine the experimental conditions, which are shown in Table 1. Specimens C_1 and C_2 were subjected to the failure test. The influence of axial pressure was tested by adding an axial load on C_3. The mass of the model car was set as 17.55 kg, 21.55 kg, and 25.55 kg. The drop heights of the model car were set as 30 cm, 80 cm, 150 cm, and 200 cm.

Table 1. Lateral impact experimental conditions.

Column Number	Test Number	Impact Mass (kg)	Drop Heights (cm)	Axial Pressure
C_1	1-1	17.55	30, 80, 150, 200	None
	1-2	21.55	30, 80, 150, 200	None
	1-3	25.55	30, 80, 150, 200	None
C_2	2-1	17.55	30, 80, 150, 200	None
	2-2	21.55	30, 80, 150, 200	None
	2-3	25.55	30, 80, 150, 200	None
C_3	3-1	17.55	30, 80, 150, 200	None
	3-2	17.55	30, 80, 150, 200	20% Pu
	3-3	17.55	30, 80, 150, 200	40% Pu
	3-4	17.55	30, 80, 150, 200	60% Pu
	3-5	17.55	30, 80, 150, 200	80% Pu

3. Results of the Impact Test

3.1. Failure Mode

Local and integral failure are possible failure modes for RCCs subjected to lateral impact loading. Furthermore, the failure mode is affected by the impact body properties, RCC parameters, and boundary conditions. Local failure refers to damage caused by an instantaneous impact force that manifests as concrete crushing in the contact area and concrete cracking and spalling in the adjacent area. The type of impact load has the greatest influence on integral failure. When subjected to an impulse load with a high peak and low holding, a component's shear stress quickly reaches failure stress, and bending deformation does not develop significantly, indicating that shear failure is the most likely mode. When a quasistatic load has a low peak and high holding, the bending failure mode is preferred because it allows a component to deform effectively.

There are several explanations for the distinction between RCC impact failure mode and static load failure mode. According to the inertial effect theory, the main reason for the change in failure mode is the inertia response hysteresis of the adjacent impact region under the impact. Another theory proposes that changing failure mode is caused by the uncoordinated effect of strain rate enhancement on cross-section bending capacity and shear resistance under impact loading.

In this impact test, the damage area of C_1 is shown in Figure 6. The following stages of the C_1 failure process were identified through a video-recording analysis: (1) local concrete fell off; (2) cracking occurred in the tension zone of the model column bottom and in the impact contact position locally; (3) cracking occurred on the backside of the impact position; (4) and, in the bottom tension zone, cracks developed and penetrated to form a plastic hinge. Although the impact process of C_1 showed local damage in the impact contact area, the ultimate failure mode was the crack penetration of the bottom tension zone, which was an integral failure.

The damage area of C_2 is shown in Figure 7. The following are brief explanations of the failure process: (1) the concrete fell off in the impact contact zone; (2) cracks in the contact zone and the tension zone at the column bottom were developed; and (3) cracks in the contact zone developed to produce plastic hinges. Despite the development of cracks in the tension area at the bottom, the final failure mode was the formation of a plastic hinge via the local fracture.

3.2. Strain Response

The primary factor affecting the model columns' strain response was the impact energy. The strain time history of the rebar and concrete of C_1, along with various drop heights, is shown in Figure 8. The contact between the car and the RCC was very brief, as can be seen from the strain time history. Then, the model car rebounded, and the model column oscillated freely to absorb the impact energy. The strain time history demonstrated that

the concrete's strain peak was positively connected with the model car's drop height. The strain peak of the rebar grew as the drop height increased.



(a)



(b)



(c)



(d)

Figure 6. Damage area of C_1: (a) concrete falling off at the impact contact position; (b) concrete cracking at the impact contact position; (c) concrete cracking at the column bottom; and (d) concrete cracking at the backside of the contact position.



(a)



(b)

Figure 7. Damage area of C_2: (a) concrete cracks at the impact contact position and (b) concrete cracks at the backside of the contact position.

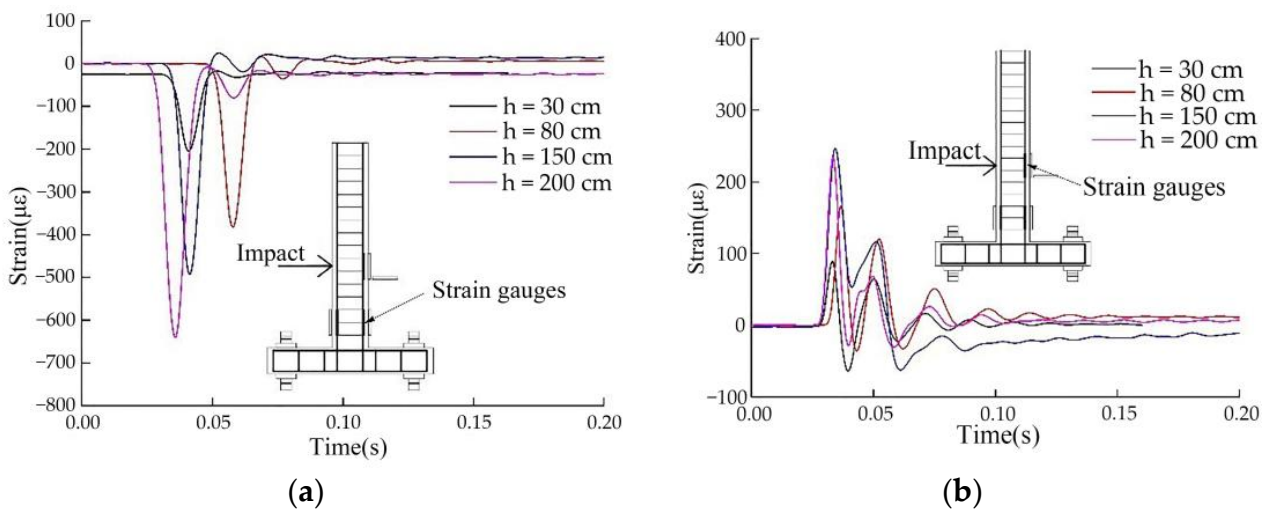


Figure 8. Strain time history of rebar and concrete at the column bottom: (a) strain time history of concrete and (b) strain time history of rebar.

The inertia effect, stress wave propagation effect, and dynamic behavior of the materials were three factors that needed to be considered in the impact problem. Due to the inertia effect, the deformation and force mode of the reinforced concrete column under impact were significantly different from the static effect. At the beginning of the impact, the rebar and concrete deformation were not coordinated. The instantaneous contact between the rebar and concrete was in an inertial constraint relationship due to the inertia effect and the bonding effect between the rebar and concrete. The highest strain of the rebar trailed the peak strain of the concrete. Eventually, when the impact energy steadily decreased, the deformation of the concrete and rebar began to cooperate. The strain time history of the concrete and rebar at the same location in C_1 is shown in Figure 9. As the drop height rose, the stress on the rebar and concrete grew.

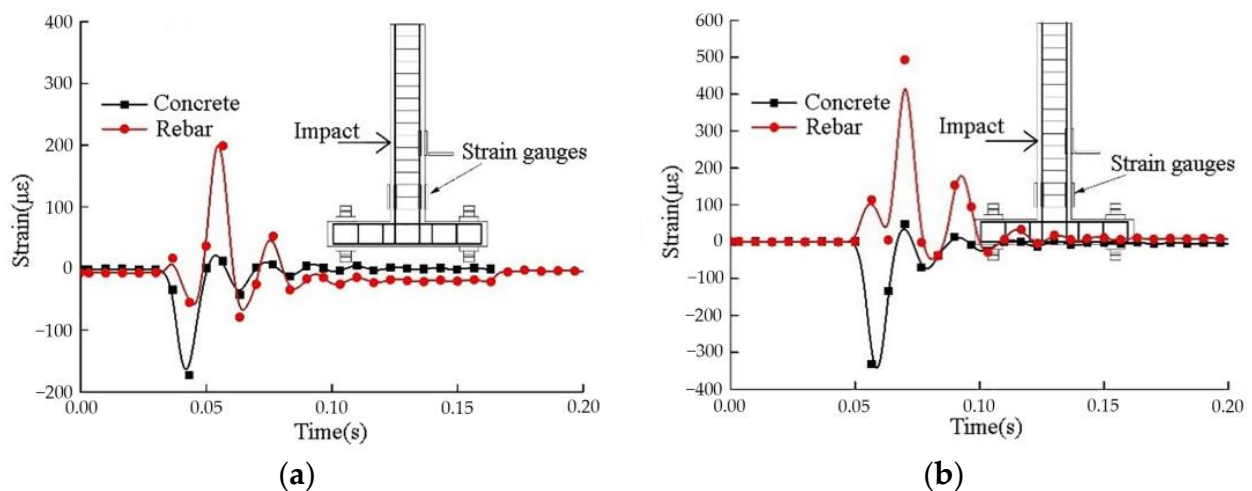


Figure 9. Inertial restraint effect during impact: (a) drop height = 30 cm and (b) drop height = 80 cm.

The impact mass was modified by adding weight to the model car, with a single ballast weighing 2 kg. The strain time history of the concrete when the drop height was 1.5 m is shown in Figure 10. As can be seen from the picture, when the mass of the model car increased by 22.8% and 45.6%, the extreme concrete strain at the same position increased by 22.5% and 42.3%, respectively.

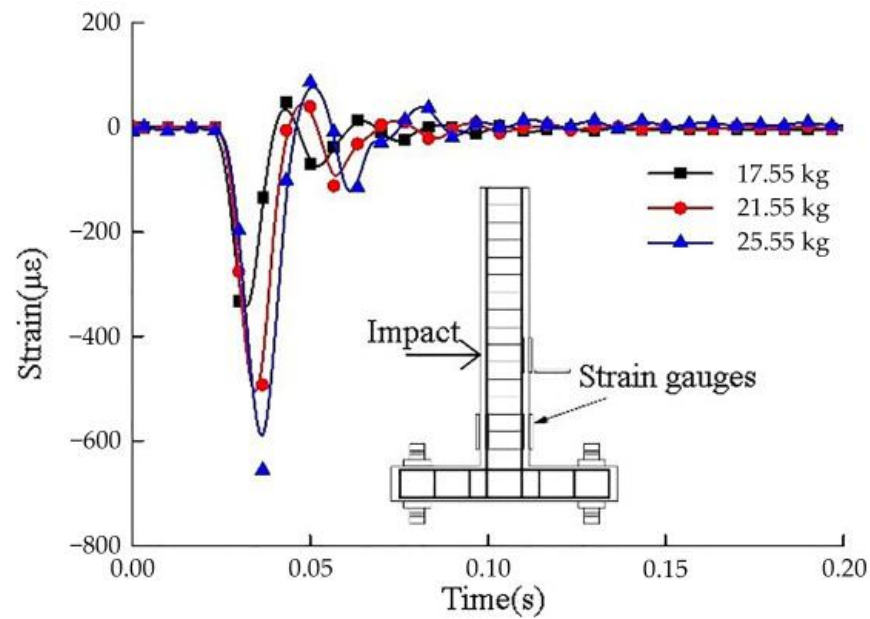


Figure 10. Strain time history of concrete with different impact masses.

Additionally, the effect of axial pressure on RCC lateral impact performance was investigated. Prior to the impact test, a pre-load of 50 kN of axial force was applied. After the load was stabilized, the car was gently pushed to hit the model column to test the effectiveness of the acquisition channel.

The strain time history of the concrete of C_3 under no axial pressure is shown in Figure 11. The peak strain rose as the drop height increased. Figure 12 depicts the strain time history of the concrete of C_3 when the axial compression ratio was equal to 0.2. The overall tendency was that, as the drop height grew, so did the strain response of the concrete. Unfortunately, no damaging load was applied due to safety concerns. The axial compression ratio was studied using numerical modeling to see how it influenced the lateral impact failure mechanism of RCCs.

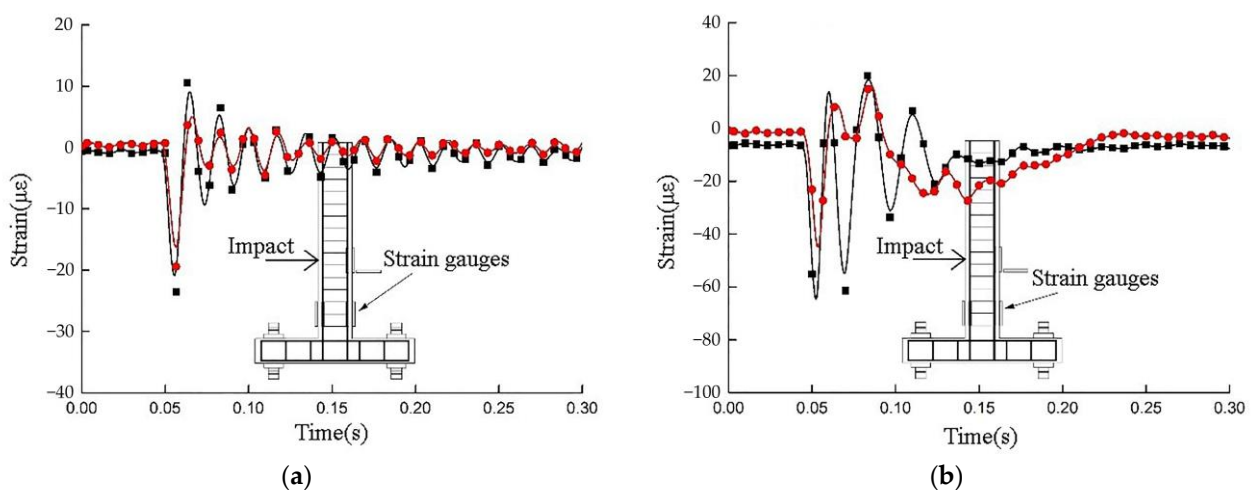


Figure 11. Strain time history of concrete of C_3 with nonaxial compression: (a) drop height = 30 cm and (b) drop height = 200 cm.

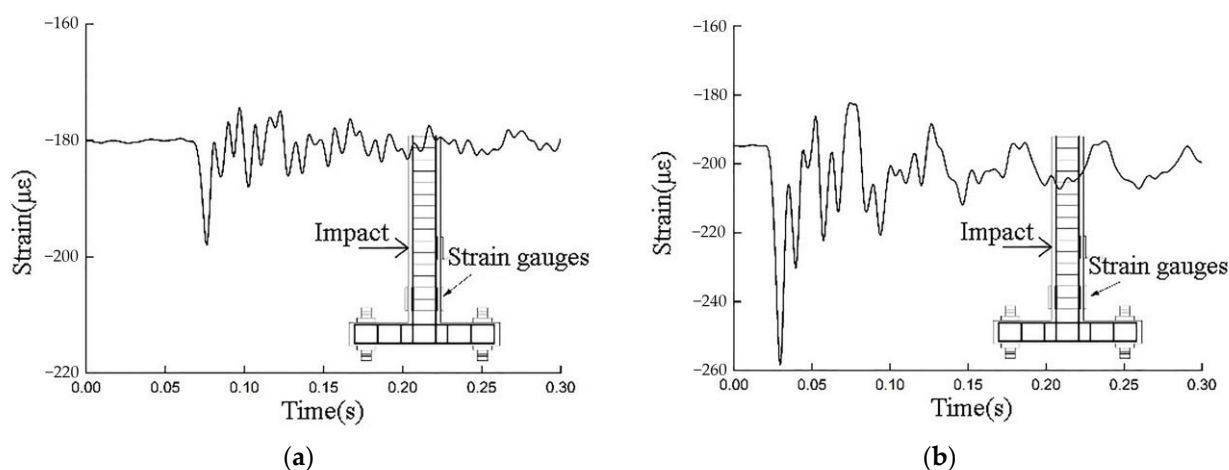


Figure 12. Strain time history of concrete of C_3 when axial compression ratio was 0.2: (a) drop height = 30 cm and (b) drop height = 200 cm.

These test results demonstrate how the response and failure mode of RCCs under lateral impact loading was affected by impact velocity, impact mass, and axial pressure. Further analysis was performed next using numerical simulation methods for additional parametric research.

4. Nonlinear Numerical Simulation

4.1. Finite Element Model

The present impact test data of the reinforced concrete members is still scarce since the impact test had a high need for the collecting device, a high safety risk, and high expense. High-precision modeling of the failure processes of reinforced concrete structures under impact is now achievable due to the development of contact algorithms and constitutive material damage models. The impact response and damage failure process analyses of complex structures are often carried out using a numerical technique once the reliability of a numerical simulation tool has been confirmed by a limited number of tests. The finite element method is gradually becoming an important aid to study impact on reinforced concrete structures.

A face-to-face contact algorithm based on a penalty function was used to simulate the impact process between the car and RCCs in this study. The bond slip between the concrete and rebar during the impact process was ignored. The finite element model of a specimen is shown in Figure 13. The constraints in the experiments were modeled by constraining the freedom of the concrete caps, and progressive grid density was used to discretize the concrete cap element. The model car was simplified in the finite element model. Since the impact contact process lasted for a short time, the effects of the car tires and track friction on the impact process were not considered.

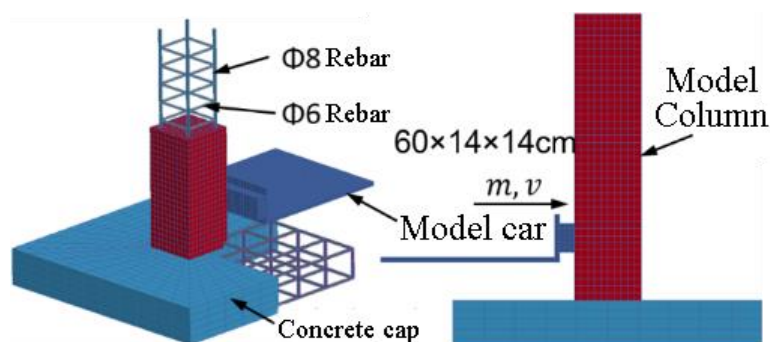


Figure 13. Finite element model of specimen.

The material model of the column and the concrete cap used in the simulation was an elastoplastic damage continuous face cap model [23–25]. In the absence of detailed meridian strength parameters, cap parameters, position parameters, and material damage parameters, the model parameters were interpolated values corresponding to the strength of the concrete in the experiment. The material model of the rebar was an elastoplastic follow-up strengthening model, and the steel yield stress rate correlation was considered using the Cowper–Symonds formula [26].

4.2. Results and Discussions

The boundary conditions and local contact conditions were improved to reproduce the impact test conditions. By contrasting the strain time history in the simulation with the experimental data, the reasonability and accuracy of the numerical simulation approach were confirmed. Figures 14 and 15 show the simulation and experimental results of the strain data of C_1 under different drop heights. Regardless of the changing model boundary conditions and damping parameters of the impact system, the numerical simulation values of strain could be well-matched with the experimental results in the curve waveform characteristics and the attenuation law. The cause of the strain peak difference may be the transient edge contact conditions in the experiment.

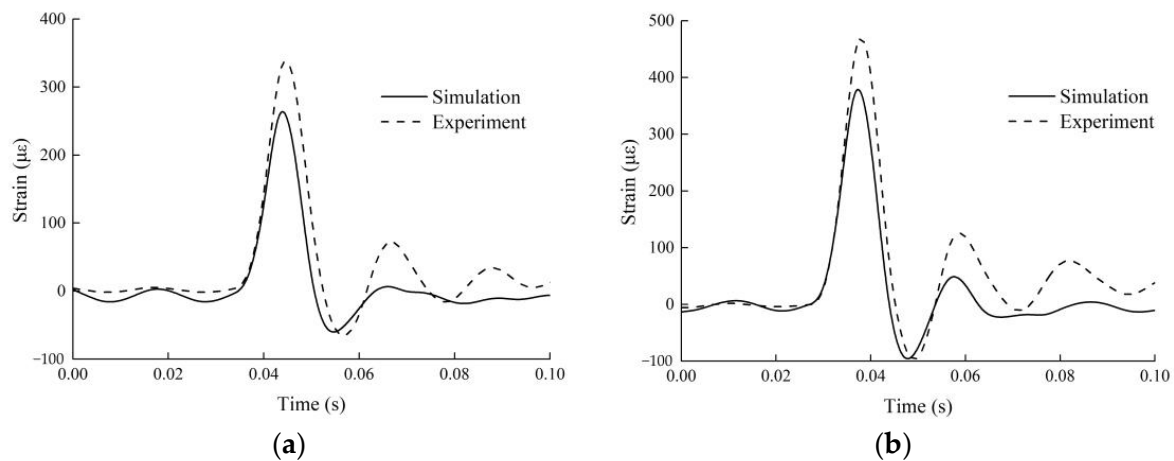


Figure 14. Strain comparison of rebar in C_1: (a) drop height = 30 cm and (b) drop height = 80 cm.

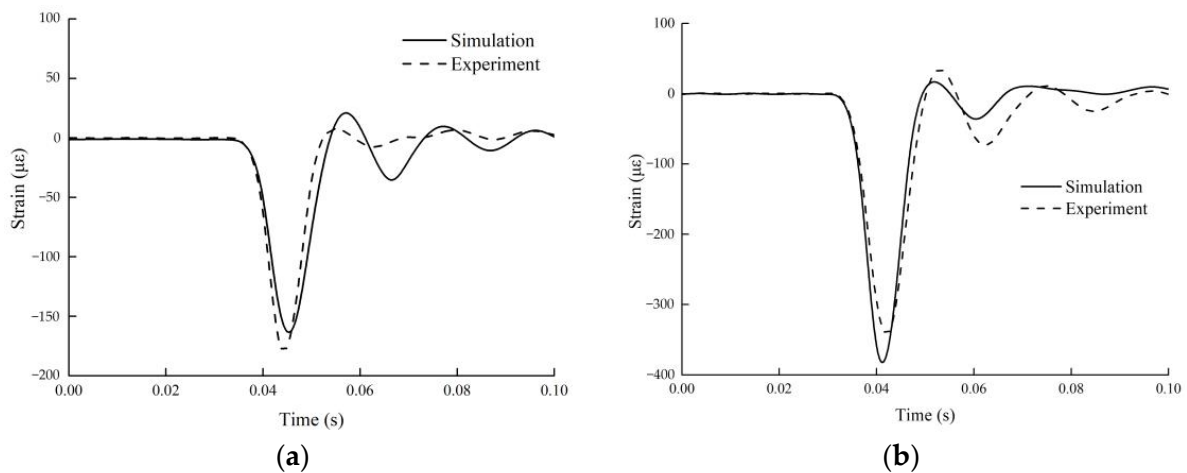


Figure 15. Strain comparison of concrete on backside of C_1: (a) drop height = 30 cm and (b) drop height = 80 cm.

In the impact test, two different types of failure modes occurred in RCC specimens with different slenderness ratios. The dominant failure mode of C_1 was that the bottom

was subjected to tensile cracking and the entire model column was rotated around the bottom, which was an overall failure mode. The dominant failure mode of C_2 was that the local crack in the contact position formed a plastic hinge that penetrated through the contact position, which was a local failure mode. The numerical calculations of the RCC failure process and the outcomes of the experiments were identical.

The comparison of the final deformation of the RCCs is shown in Figure 16. The impact deflection of the two model columns was different under the same drop height. The deflection curve of C_1 showed that there was a plastic hinge around the bottom. The deflection curve of C_2 showed deformation in the area adjacent to the impact position. In addition, due to the reverse displacement of the top of the model column, the impact area was formed on the backside of the model column. The failure modes of the columns obtained by numerical simulation agreed well with the experimental results.

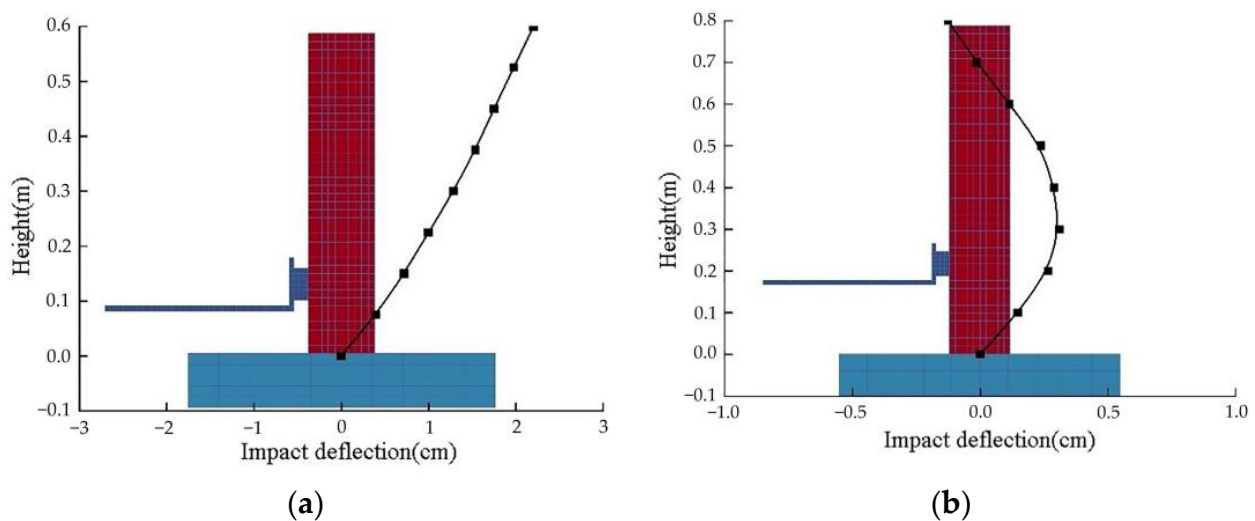


Figure 16. Comparison of RCC failure mode: (a) impact deflection curve of C_1 and (b) impact deflection curve of C_2.

5. Parametric Analysis

5.1. Effect of Impact Energy

By altering the model car's mass and drop height, the effect of impact energy was evaluated. Figure 17 shows damage cloud maps of model columns at different impact speeds. The main damage areas were the backside inertial tension area and the bottom area. As the impact speed increased, the damage area expanded significantly.

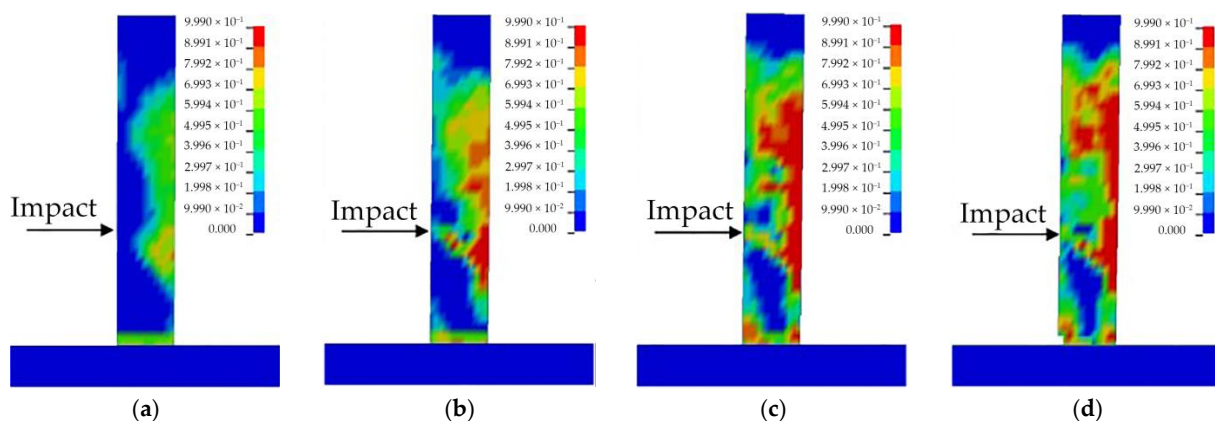


Figure 17. Comparison of damage at different impact speeds: (a) $v = 2.425$ m/s; (b) $v = 3.960$ m/s; (c) $v = 5.422$ m/s; (d) $v = 6.260$ m/s.

Impact body mass and impact velocity are the two most important factors affecting the contact interface force [27]. Equivalent static impact loads are expressed mostly as a function of impact mass and impact velocity [1]. Figure 18 shows the relationships among peak contact interface force, impact velocity, and impact mass.

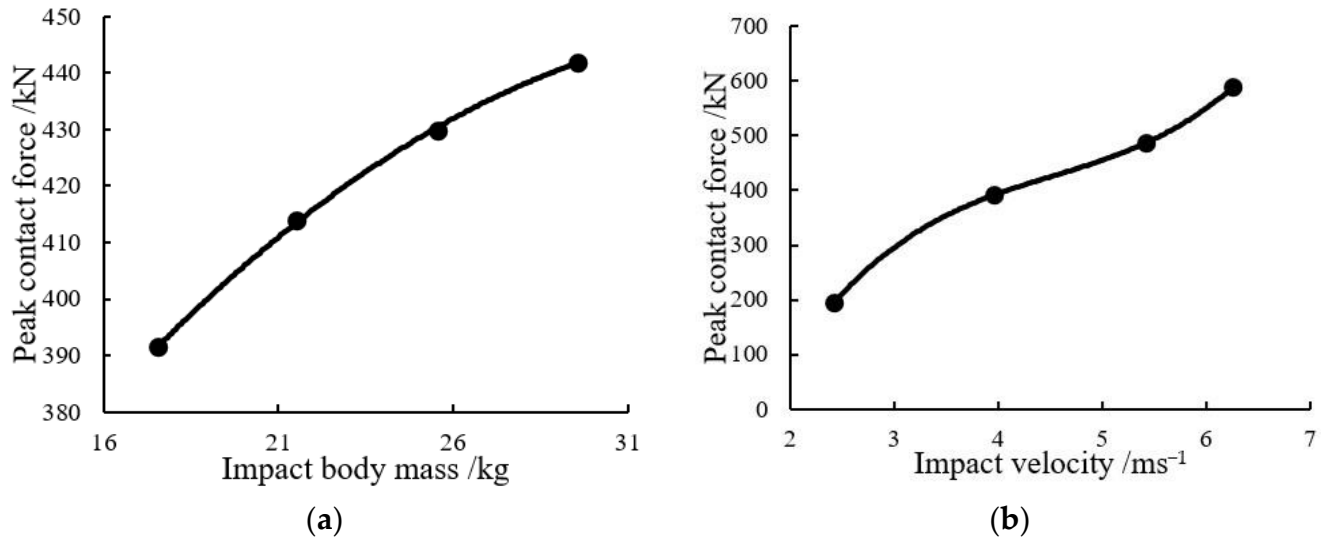


Figure 18. Relationships among peak contact force, impact mass, and impact velocity: (a) relationship between peak contact force and impact mass; (b) relationship between peak contact force and impact velocity.

As impact mass and velocity rose, so did impact impulse and peak contact interface force. The link between the contact interface force peak and impact mass could best be matched by a quadratic polynomial in the set of data points examined in this study, whereas the relationship between the contact interface force peak and impact velocity was best-suited by a cubic polynomial.

5.2. Effect of Reinforcement Ratio

To investigate the effects of various reinforcement ratios on the performance of RCCs under lateral impact loading, the longitudinal reinforcement and stirrup diameters were altered.

Along with an increase in longitudinal reinforcement diameter, there was a change in local contact stiffness and an increase in peak contact interface force. Peak horizontal displacement and residual column top displacement decreased with an increase in the longitudinal reinforcement ratio. Figure 19 shows the comparison of the damage to model columns using different longitudinal rebars under the same impact energy ($m = 17.55$ kg, $v = 3.960$ m/s). The impact damage zone was the impact backside inertia effect tension zone, and the increase in longitudinal reinforcement size significantly reduced the impact damage.

The local contact stiffness rose with the stirrups' increasing diameter. The increase in stirrup diameter could significantly reduce the impact deformation of the RCCs. Figure 20 compares the displacement of column tops with various reinforcing ratios. As the diameter of the stirrup increased, the maximum displacement and the residual deformation of the RCCs were reduced. The lateral impact resistance of the RCCs could be increased by increasing the stirrup reinforcement ratio.

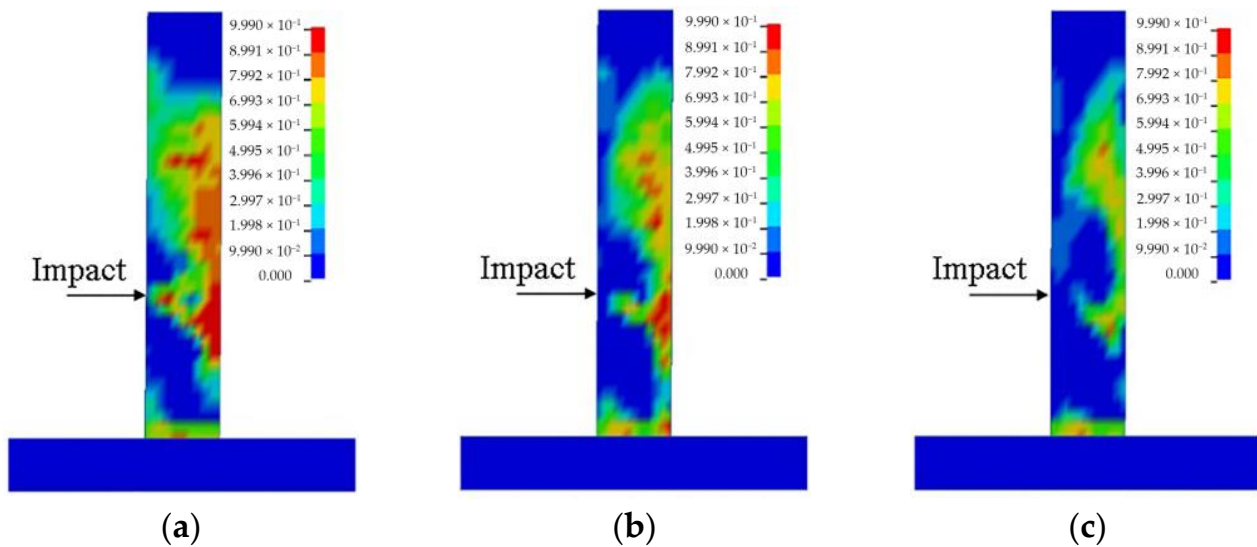


Figure 19. Comparison of impact damage to columns with different longitudinal reinforcement ratios: (a) $\Phi 6$ longitudinal rebar; (b) $\Phi 12$ longitudinal rebar; (c) $\Phi 18$ longitudinal rebar.

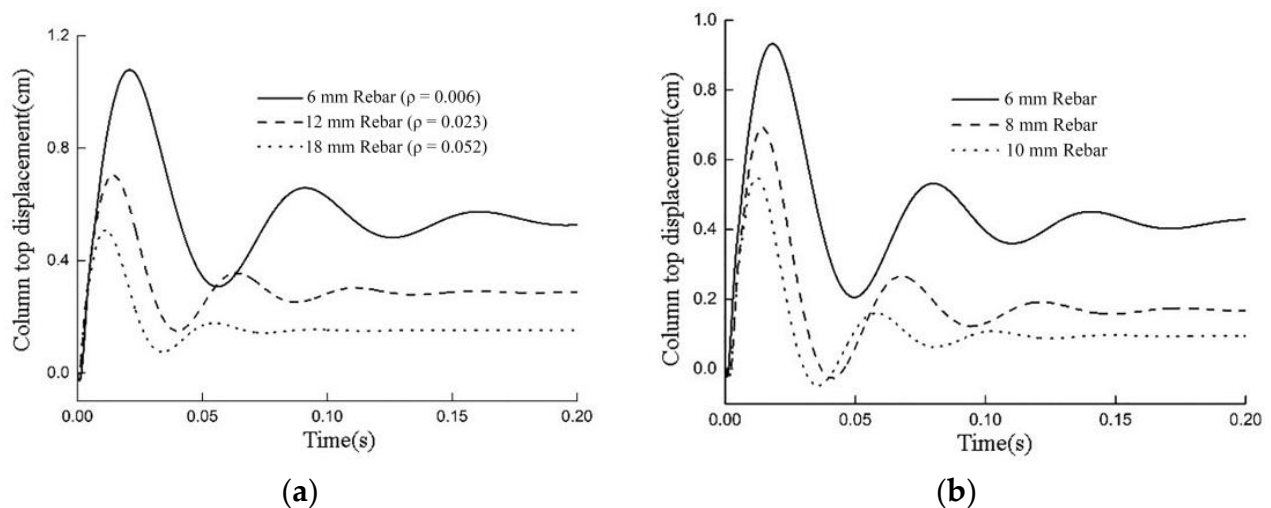


Figure 20. Relationship between column top displacement and reinforcement ratio: (a) relationship between column top displacement and longitudinal reinforcement; (b) relationship between column top displacement and stirrup.

5.3. Effect of Concrete Strength Grade

Two factors needed to be taken into account when analyzing how the increase in axial compressive strength affected RCC impact resistance. To begin, the model column entered the plastic damage region at the same load level as the concrete strength rose, somewhat enhancing the model column's impact resistance. For instance, the dynamic yield strength of the concrete under the impact load was somewhat increased as a result of the correlation with concrete strength rate under the impact load. The relationship between the concrete strength grade and the concrete strength increase coefficient showed that lower strength concrete had a larger power increase coefficient. Figure 21 shows the relationship between impact deflection of model columns and concrete strength.

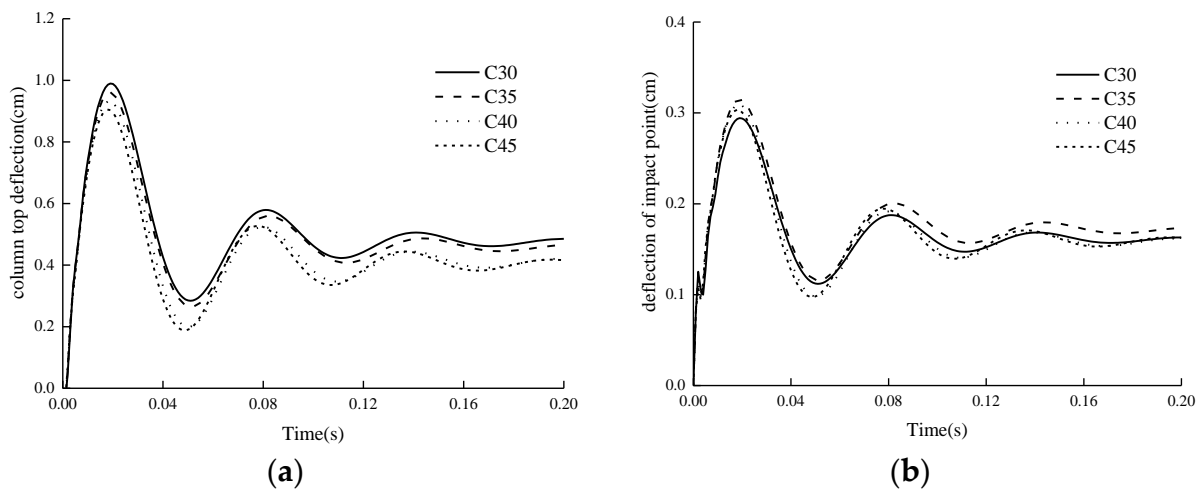


Figure 21. Impact deflection of model columns with different concrete strengths: (a) relationship between column top deflection and concrete strength; (b) relationship between deflection of impact point and concrete strength.

Figure 22 is an equivalent damage cloud diagram of the continuous face cap model of RCC. The impact damage area of the RCC only slightly lowered as concrete strength grade rose. Due to the correlation between the dynamic strain rate effect of concrete and concrete strength grade, the improvement in concrete strength grade under the analysis conditions of this paper limited the improvement in the lateral impact resistance of the model column from the perspectives of overall impact and local damage.

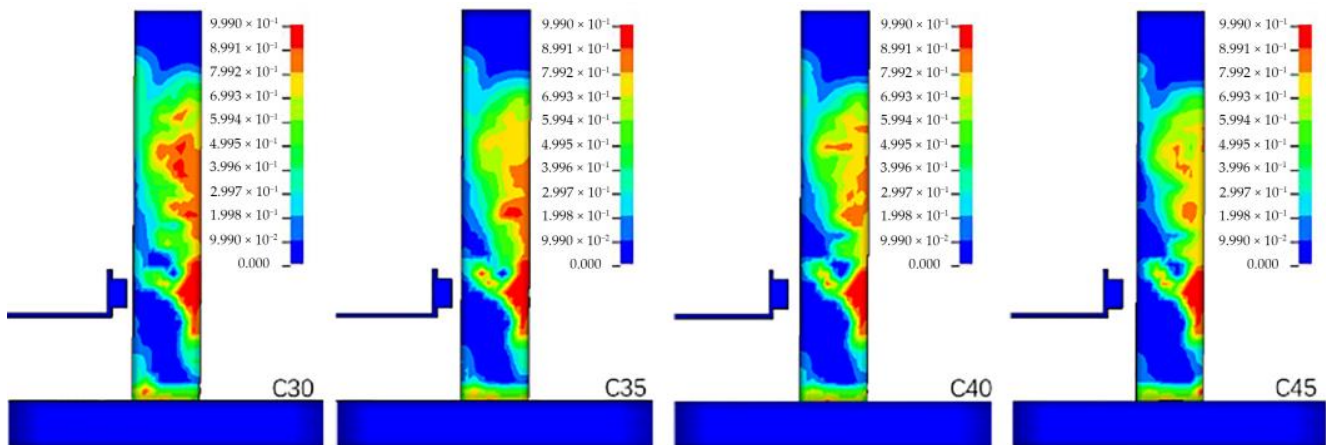


Figure 22. Influence of concrete strength grade on impact damage of model column.

5.4. Effect of Slenderness Ratio

The influence of the slenderness ratio of RCCs on the impact effect was evaluated using columns with different heights. The heights of the three models were 0.6 m, 0.8 m, and 1.0 m respectively. The boundary of the models was the lower end consolidation, and the top was unconstrained. The fine ratios were 29.7, 39.6, and 49.5, respectively. The impact position was the midpoint of the column. The impact body mass was 17.55 kg, and the impact contact instantaneous velocity was 3.960 m/s. The model column sections and reinforcement were the same as C_1. The finite element models are shown in Figure 23. The constitutive structures of the concrete and rebar were the same as in the previous analysis. The coupling degree of gravity was used to simulate the co-deformation relationship between rebar and concrete. The initial stress of gravity was pre-added using the dynamic relaxation method, and the influence of gravity was simulated with body acceleration.

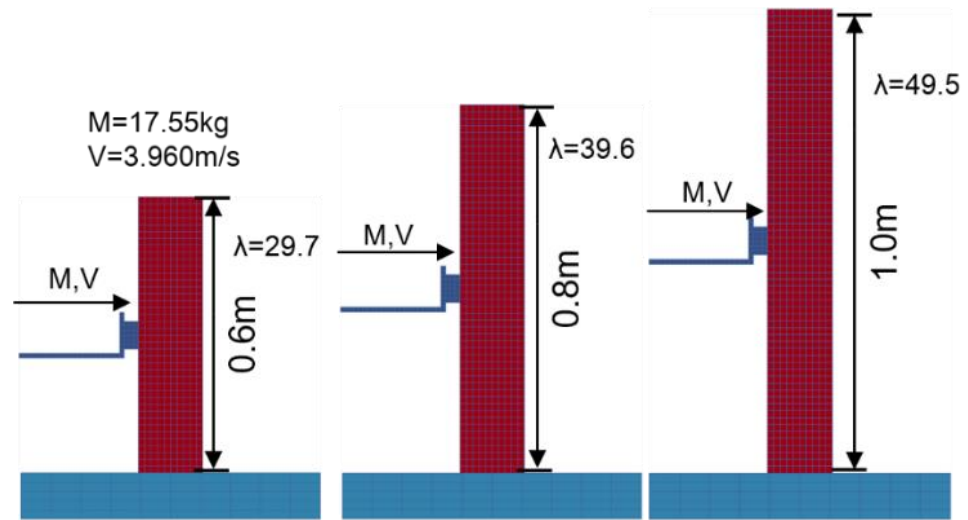


Figure 23. Finite element model of columns with different slenderness ratios.

As column height increased, the maximum contact interface force also increased. The corresponding peaks were 16.134 kN, 17.197 kN, and 18.192 kN, respectively. Figure 24 shows the comparison of the displacement angles of RCCs with different slenderness ratios. The top displacement extreme value was positively correlated with the column height. The maximum lateral displacements of the column tops were 7.6 cm, 13.1 cm, and 22.2 cm, respectively. Under the condition of midpoint impact of the RCCs, the displacement angle was positively correlated with the slenderness ratios of the RCCs.

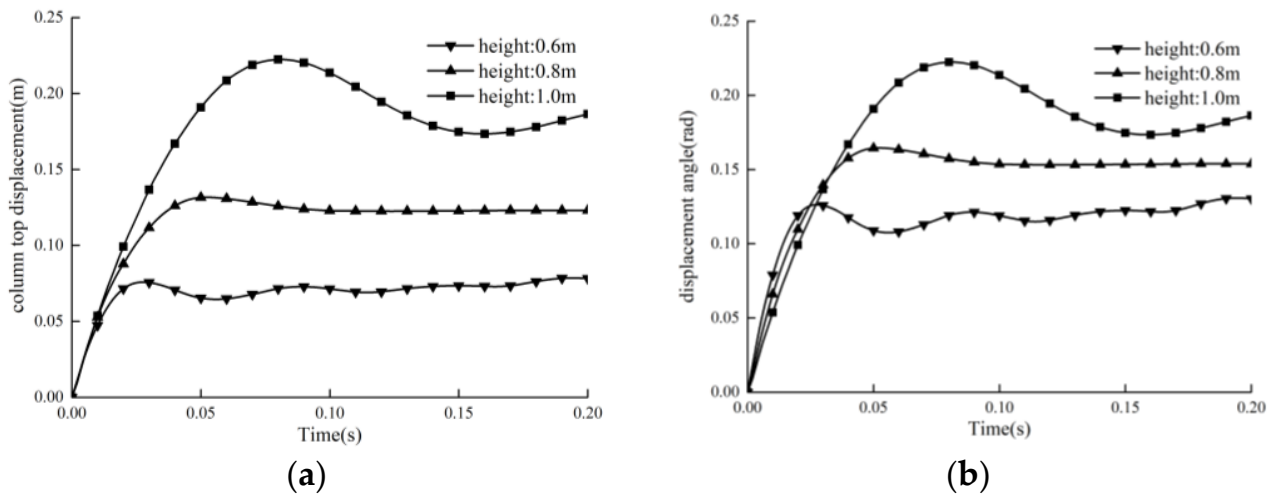


Figure 24. Comparison of RCCs with different slenderness ratios: (a) comparison of column top displacement; (b) comparison of column displacement angle.

5.5. Effect of Axial Compression Ratio

Two perspectives can be used to analyze how the axial compression ratio affects the impact resistance of RCCs. On the one hand, the impact resistance and damage failure mode of a column section are impacted by the second-order effect of axial force. On the other hand, the contact interface force time history is somewhat impacted by variations in the axial compression ratio and the contact stiffness between the impact body and the column impact contact area. However, there are differences in existing research conclusions. He Su et al. [28] used an MTS dynamic-loading device to carry out the multipoint loading of RCC lateral impact loads and studied the effect of the axial compression ratio. The specimen lateral displacement increased with increase in the axial compression ratio at the

same loading rate. Huijia Wang [29] conducted a shear failure test of 30 reinforced concrete beams. It was concluded that the shear resistance varied with the axial compression ratio. When the axial compression ratio was less than 0.4–0.5, the axial pressure improved the shearing capacity. Xiaozhen Zhou [30] conducted a shear failure test of 18 RCCs. The findings showed that the shear strength rose with an increase in the axial compression ratio when the ratio was smaller than 0.8. The current design standards do not harmonize axial force and section shear capacity. In conclusion, different studies have reached different results about the relationship between the axial compression ratio and the lateral impact behavior of RCCs.

This section compares how the axial compression ratio affected RCC behavior under lateral impact loading. The column size was 80 cm × 14 cm × 14 cm (Figure 25). The axial compression ratios were 0, 0.2, 0.4, 0.6, and 0.8. In the five working conditions, the impact mass of the model car was 17.55 kg, and the impact velocity analyses of impact strength were 2 m/s and 4 m/s. The axial initial pressure in the analysis was loaded using the dynamic relaxation method.

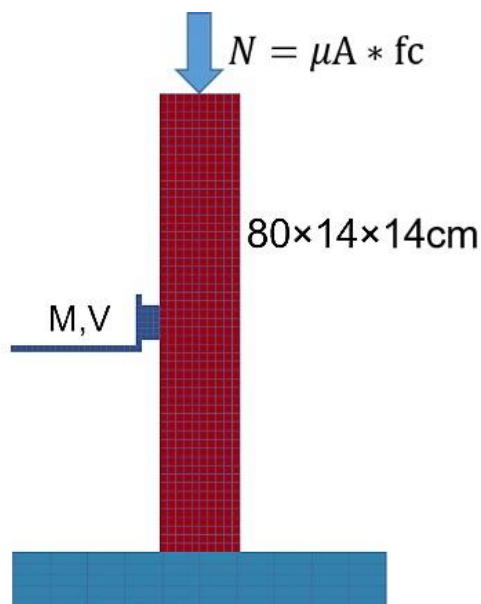


Figure 25. Finite element model considering influence of axial pressure ratio.

The relationship between peak contact force and axial pressure ratio is given in Figure 26. The peak contact interface force increased with the increase in the axial compression ratio under the same impact energy. In addition, the peak contact interface force at the same axial pressure ratio and the contact holding time increased with the increase in the impact speed.

The relationship between column top displacement and axial pressure ratio is given in Figure 27. With an increase in the axial compression ratio, the column top displacement decreased. With an increase in the axial compression ratio in the scenario of higher impact velocity, the displacement of the top of the column increased more quickly. The damage area and failure mode of the impact scenario model did not differ noticeably, and the damage area of the model column was primarily on the collision side of the root. The peak contact interface force increased to a certain extent due to the stress stiffness caused by the increased axial compression ratio, which also reduced the impact deformation of the RCCs.

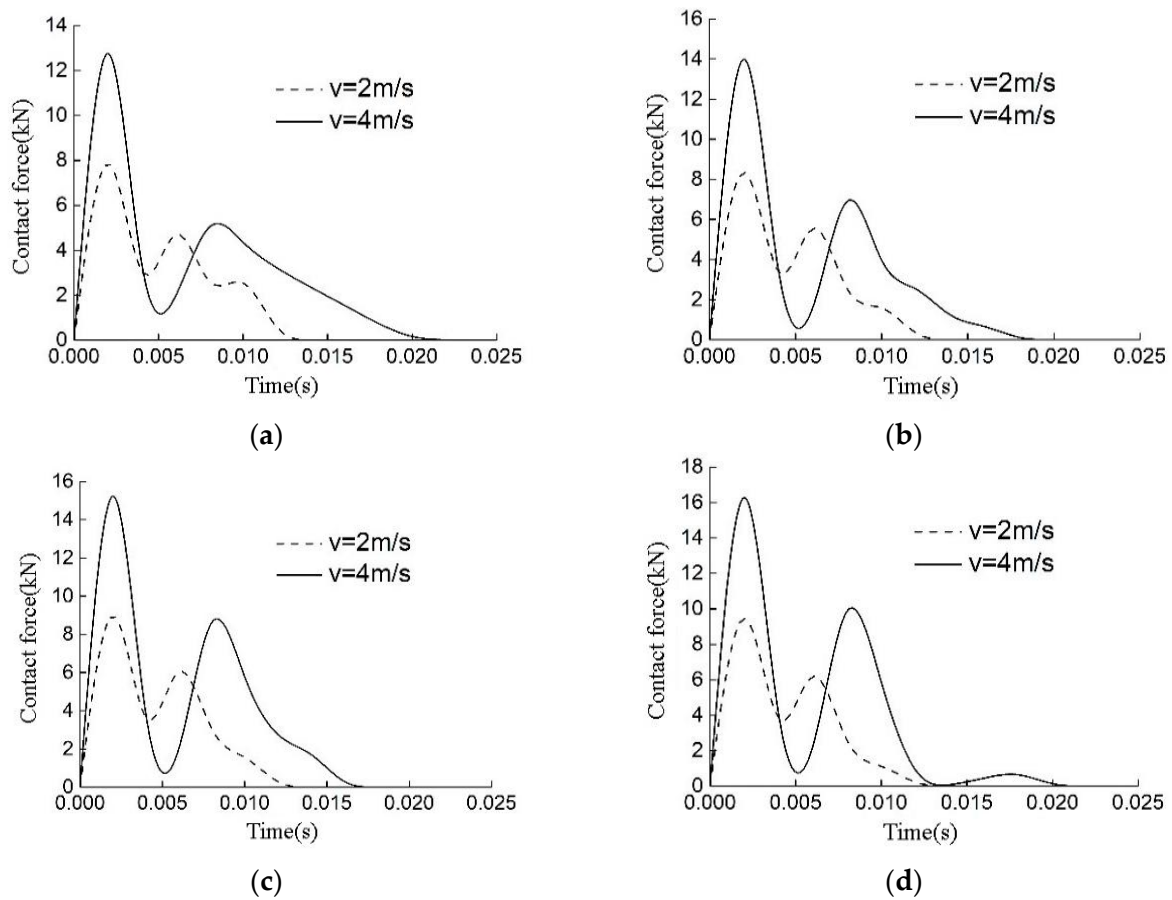


Figure 26. Relationship between peak contact force and axial pressure ratio: (a) axial compression ratio = 0.2; (b) axial compression ratio = 0.4; (c) axial compression ratio = 0.6; (d) axial compression ratio = 0.8.

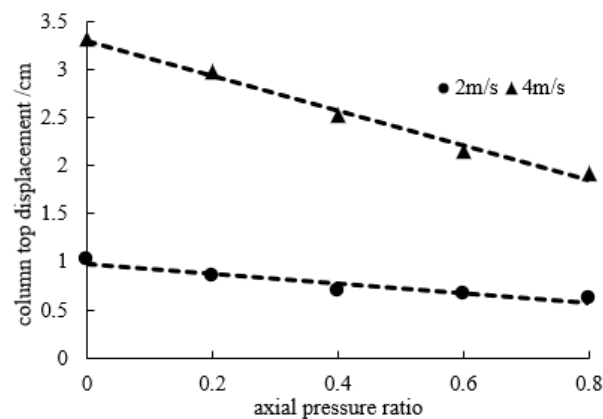


Figure 27. Relationship between column top displacement and axial pressure ratio.

6. Conclusions

Experimental and numerical studies were conducted to investigate the performance and failure mode of RCCs under lateral impact loading. The findings of this study led to the following conclusions:

1. The findings of the impact test revealed that the impact mass and velocity were the most important elements influencing the dynamic strain response of the model columns. When the mass of the model car increased by 22.8% and 45.6%, the extreme concrete strain

at the same position increased by 22.5% and 42.3%, respectively. The extreme value of dynamic strain was positively correlated with the impact mass and impact velocity.

2. The results indicated that the plastic deformation and the impact damage of the model columns significantly reduced as the longitudinal reinforcement ratio increased. The impact deformation increased with the increase in column height, and the energy conversion time was extended during the contact process.

3. Since the strength increase coefficient (DIF) of the concrete material was related to the strength grade of the concrete, concrete with a lower strength grade could have greater dynamic load strength under the same strain rate. Raising the concrete strength at the experimental impact strain rate improved a model column's impact resistance only marginally. As the slenderness ratio of the model column increased (the section was constant and the column height increased), the lateral impact failure mode of the model column did not change significantly.

4. The effect of the axial pressure ratio on the model column lateral impact resistance must be examined by integrating the model column action–resistance relationship and deformation capacity. The enhanced axial pressure ratio's stress stiffness minimized the impact deformation of the model columns while simultaneously increasing the peak contact interface force to some extent.

These research results can provide a reference for impact-resistant design and make it easier to more accurately evaluate the performance of RCCs under lateral impact loading.

Although RCCs with axial forces under lateral impact loading were studied in this work using a self-designed experimental facility, the mechanism of the influence of axial forces on the impact-bearing capacity of RCCs remains uncertain. The authors recommend that extensive experimental work should be conducted when conditions allow, as present relevant experimental data are still scant. Micro-level concrete mechanism studies can assist in understanding the influence of axial forces on the lateral impact behavior of RCCs. Investigations were only performed at the member level in this study, but further studies at the structural level can be conducted in the future.

Author Contributions: Conceptualization, A.C.; methodology, A.C. and Y.L.; validation, A.C. and R.M.; formal analysis, Y.L. and X.Z.; investigation, X.Z.; data curation, Y.L. and X.Z.; writing—original draft preparation, Y.L.; writing—review and editing, R.M.; supervision, A.C.; funding acquisition, A.C. All authors have read and agreed to the published version of the manuscript.

Funding: This research was funded by the National Natural Science Foundation of China (No. 52238005) and the National Key Research and Development Program of China (No. 2021YFF0501003).

Data Availability Statement: Data sharing not applicable.

Conflicts of Interest: The authors declare no conflict of interest. The funders had no role in the design of the study; in the collection, analyses, or interpretation of data; in the writing of the manuscript; or in the decision to publish the results.

References

1. Buth, C.E.; Williams, W.F.; Brackin, M.S.; Lord, D.; Geedipally, S.R.; Abu-Odeh, A.Y. *Analysis of Large Truck Collisions with Bridge Piers: Phase 1, Report of Guidelines for Designing Bridge Piers and Abutments for Vehicle Collisions*; Texas Transportation Institute: College Station, TX, USA, 2010.
2. Lu, Y.E.; Zhang, L.M. Progressive collapse of a drilled-shaft bridge foundation under vessel impact. *Ocean. Eng.* **2013**, *66*, 101–112. [[CrossRef](#)]
3. Abrams, D.A. Effect of rate of application of load on the compressive strength of concrete. *Proc. ASTM* **1956**, *17*, 364–377.
4. Hughes, B.P.; Watson, A.J. Compressive strength and ultimate strain of concrete under impact loading. *Mag. Concr. Res.* **1978**, *30*, 189–199. [[CrossRef](#)]
5. John, R.; Shah, S.P. Effects of high strength and rate of loading on fracture parameters of concrete. In *Fracture of Concrete and Rock, Proceedings of the SEM-RILEM International Conference, Houston, TX, USA, 17–19 June 1987*; Springer: New York, NY, USA, 1987; pp. 35–52.
6. Ross, C.A.; Thompson, P.Y.; Tedesco, J.W. Split-Hopkinson pressure-bar tests on concrete and mortar in tension and compression. *ACI Mater. J.* **1989**, *86*, 475–481.

7. Bischoff, P.H.; Perry, S.H. Compressive behaviour of concrete at high strain rates. *RIELM Mater. Struct.* **1991**, *24*, 425–450. [[CrossRef](#)]
8. Bazant, Z.P.; Gu, W.H.; Faber, K.T. Softening reversal and other effects of a change in loading rate on fracture of concrete. *ACI Mater. J.* **1995**, *92*, 3–9.
9. Kishi, N.; Mikami, H.; Matsuoka, K.G.; Ando, T. Impact behavior of shear-failure-type RC beams without shear rebar. *Int. J. Impact Eng.* **2002**, *27*, 955–968. [[CrossRef](#)]
10. Fujikake, K.; Li, B.; Soeun, S. Impact response of reinforced concrete beam and its analytical evaluation. *J. Struct. Eng.* **2009**, *135*, 938. [[CrossRef](#)]
11. Pham, T.M.; Hao, H. Plastic hinges and inertia forces in RC beams under impact loads. *Int. J. Impact Eng.* **2017**, *103*, 1–11. [[CrossRef](#)]
12. Jahami, A.; Temsah, Y.; Khatib, J.; Sonebi, M. Rehabilitation of reinforced concrete slabs damaged by impact loading using swimmers as shear reinforcement. *Mater. Today Proc.* **2022**, *58*, 1251–1257. [[CrossRef](#)]
13. Mingyang, W.; Derong, W.; Chunming, S. A calculation method of reinforced concrete beam under low velocity impact. *Acta Armamentarii* **2006**, *27*, 399–405.
14. Jiang, H.; Wang, X.; He, S. Numerical simulation of impact tests on reinforced concrete beams. *Mater. Des.* **2012**, *39*, 111–120. [[CrossRef](#)]
15. Thilakarathna, H.M.I.; Thambiratnam, D.P.; Dhanasekar, M.; Perera, N. Numerical simulation of axially loaded concrete columns under transverse impact and vulnerability assessment. *Int. J. Impact Eng.* **2010**, *37*, 1100–1112. [[CrossRef](#)]
16. Li, T.; Cong, Z.; Hao, W.; Xinhua, F. Dynamic response and failure modes of RC columns under impact. *Eng. Mech.* **2013**, *30*, 150–155.
17. Bertrand, D.; Kassem, F.; Delhomme, F.; Limam, A. Reliability analysis of an RC member impacted by a rockfall using a nonlinear SDOF model. *Eng. Struct.* **2015**, *89*, 93–102. [[CrossRef](#)]
18. Cai, J.; Ye, J.B.; Chen, Q.J.; Liu, X.; Wang, Y.Q. Dynamic behaviour of axially-loaded RC columns under horizontal impact loading. *Eng. Struct.* **2018**, *168*, 684–697. [[CrossRef](#)]
19. Zhang, X.; Hao, H.; Li, C.; Van Do, T. Experimental study on the behavior of precast segmental column with domed shear key and un-bonded Post-Tensioning tendon under impact loading. *Eng. Struct.* **2018**, *173*, 589–605. [[CrossRef](#)]
20. Fan, W.; Liu, B.; Huang, X.; Sun, Y. Efficient modeling of flexural and shear behaviors in reinforced concrete beams and columns subjected to low-velocity impact loading. *Eng. Struct.* **2019**, *195*, 22–50. [[CrossRef](#)]
21. Yilmaz, T.; Kiraç, N.; Anil, Ö. Experimental investigation of axially loaded reinforced concrete square column subjected to lateral low-velocity impact loading. *Struct. Concr.* **2019**, *20*, 1358–1378. [[CrossRef](#)]
22. Zhao, W.; Qian, J. Resistance mechanism and reliability analysis of reinforced concrete columns subjected to lateral impact. *Int. J. Impact Eng.* **2020**, *136*, 103413. [[CrossRef](#)]
23. Murray, Y.D.; Abu-Odeh, A.Y.; Bligh, R.P. *Evaluation of LS-DYNA Concrete Material Model 159*; Federal Highway Administration, Office of Research, Development, and Technology: Washington, DC, USA, 2007.
24. Halquist, J. *LS-DYNA Keyword User's Manual, Version 971*; Livermore Software Technology Corporation: Livermore, CA, USA, 2007.
25. Kong, X.; Fang, Q.; Wu, H.; Peng, Y. Numerical predictions of cratering and scabbing in concrete slabs subjected to projectile impact using a modified version of HJC material model. *Int. J. Impact Eng.* **2016**, *95*, 61–71. [[CrossRef](#)]
26. Cowper, G.R.; Symonds, P.S. *Strain-Hardening and Strain-Rate Effects in the Impact Loading of Cantilever Beams*; Brown University: Providence, RI, USA, 1957.
27. Chu, L.M.; Zhang, L.M. Centrifuge modeling of ship impact loads on bridge pile foundations. *J. Geotech. Geoenviron. Eng.* **2011**, *137*, 405–420. [[CrossRef](#)]
28. He, S.; Wang, X. Experimental study on lateral impact resistance of reinforced concrete columns with axial compression ratio. *J. Hebei Polytech. Univ. (Nat. Sci. Ed.)* **2011**, *33*, 117–121.
29. Wang, H. Experimental study on shear behavior of reinforced concrete short columns under compression and bending. *J. Xi'an Univ. Archit. Technol. (Nat. Sci. Ed.)* **1989**, *1*, 76–84.
30. Zhou, X. Research on Restoring Force Characteristics of Reinforced Concrete Shear Failure Column under Bending and Shearing. *J. Xi'an Univ. Archit. Technol. (Nat. Sci. Ed.)* **1992**, *3*, 235–242.

Disclaimer/Publisher's Note: The statements, opinions and data contained in all publications are solely those of the individual author(s) and contributor(s) and not of MDPI and/or the editor(s). MDPI and/or the editor(s) disclaim responsibility for any injury to people or property resulting from any ideas, methods, instructions or products referred to in the content.